



MR Imaging of Pediatric Bone Marrow¹

Brian Y. Chan, MD
Kara G. Gill, MD
Susan L. Rebsamen, MD
Jie C. Nguyen, MD, MS

RadioGraphics 2016; 36:1911-1930

Published online 10.1148/rg.2016160056

Content Codes: **MK** **MR** **PD**

¹From the Department of Radiology, University of Wisconsin School of Medicine and Public Health, American Family Children's Hospital, CSC, MC 3252, 600 Highland Ave, Madison, WI 53792-3252. Recipient of a Cum Laude award for an education exhibit at the 2015 RSNA Annual Meeting. Received March 11, 2016; revision requested April 19 and received May 9; accepted June 1. For this journal-based SA-CME activity, the authors, editor, and reviewers have disclosed no relevant relationships. Address correspondence to J.C.N. (e-mail: jiec29@gmail.com).

©RSNA, 2016

SA-CME LEARNING OBJECTIVES

After completing this journal-based SA-CME activity, participants will be able to:

- Describe the normal sequences of marrow conversion and reconversion.
- Distinguish heterogeneous red marrow from neoplastic marrow replacement.
- Recognize the more common nonneoplastic pediatric edema-like processes.

See www.rsna.org/education/search/RG.

The bone marrow is one of the largest organs in the body and is visible in every magnetic resonance (MR) imaging study. It is composed of a combination of hematopoietic red marrow and fatty yellow marrow, and its composition changes throughout life in response to normal maturation (red to yellow conversion) and stress (yellow to red reconversion). MR imaging is highly sensitive for detection of altered marrow signal intensity, and the T1-weighted spin-echo sequence provides the most robust contrast between yellow marrow and disease. Heterogeneous red marrow and red marrow hyperplasia can mimic marrow disease, but should be distinguished from neoplastic replacement (leukemia, lymphoma, primary bone sarcomas, hematogenous metastases) and expected posttreatment changes (radiation therapy, chemotherapy, colony-stimulating factor, bone marrow transplant). Nonneoplastic edema-like processes can also alter marrow signal intensity, including trauma, infection, inflammation (chronic recurrent multifocal osteomyelitis, juvenile inflammatory arthritis), altered biomechanics, and chronic regional pain syndrome. Unfortunately, MR imaging findings are often nonspecific and overlap among many of these vastly different causes. Therefore, a definitive diagnosis is reliant on a combination of imaging findings, clinical evaluation, laboratory assessment, and occasionally tissue analysis.

©RSNA, 2016 • radiographics.rsna.org

Introduction

The bone marrow is one of the largest organs in the body after bone, skin, and fat (1), and its composition changes throughout life in response to normal maturation (red to yellow conversion) and stress (yellow to red reconversion). The greatest physiologic marrow composition change occurs during infancy and childhood. Although this maturation process continues throughout adulthood, it occurs at a much slower pace.

With continued improvement in faster image acquisition times and the advantage of lack of radiation exposure, there is growing use of magnetic resonance (MR) imaging in evaluation of pediatric patients. The bone marrow is visible in every MR imaging study, often in exquisite detail. Therefore, the radiologist may be the first to detect unsuspected marrow disease, resulting in changes in patient management and outcome. At times, accurate and confident identification of marrow disease can be challenging, particularly in the pediatric population, where altered marrow signal intensity can represent normal marrow conversion, heterogeneous residual red marrow, physiologic response to stress, or true disease.

In this article, we first review the normal bone marrow: (a) its histologic composition and how it contributes to the MR imaging appearance, (b) normal red to yellow marrow conversion and its distribution based on age and location, and (c) pathognomonic locations and appearances of heterogeneous residual red marrow.

TEACHING POINTS

- Red to yellow marrow conversion occurs throughout childhood and into early adulthood. An adult pattern is finally reached at approximately 25 years of age, characterized by the distribution of the red marrow limited to the axial skeleton (skull, vertebrae, ribs, sternum, and pelvis) and proximal aspects of the appendicular skeleton (femora and humeri). This normal physiologic marrow conversion follows a predictable pattern throughout the body and within individual bones.
- Yellow to red marrow reconversion occurs in the exact reverse order, centripetally from the axial to the appendicular skeleton and within the long bones, starting in the proximal metaphysis, followed by the distal metaphysis, and finally within the diaphysis. In times of severe stress, epiphyseal marrow reconversion, marrow cavity expansion, and/or extramedullary hematopoiesis can occur. Deviation from this pattern suggests an alternative diagnosis.
- Tumors occur more commonly in the region of red marrow due to its richer vascularity and more active mitotic rates. In contrast to red marrow, which is mildly hyperintense relative to muscle on T1-weighted images, hypointensity relative to muscle has 81% accuracy for identifying an infiltrative process and hypointensity relative to intervertebral disks has 78% accuracy.
- A diverse group of nonmalignant processes can produce low T1-weighted and high fluid-sensitive signal intensity within the marrow, including trauma, infection, inflammation, altered biomechanics, and chronic regional pain syndrome. Although this imaging pattern is loosely termed *bone marrow edema*, histopathologic examination demonstrates a variable amount of hemorrhage, fibrosis, and/or necrosis in addition to fluid; therefore, it is better termed *edema-like lesion*.
- Repetitive strenuous activity can cause microtrauma to the physis due to disruption of the metaphyseal vascular supply, resulting in extension of hypertrophic chondrocytes into the metaphysis. This is most common in the shoulder of pitchers (Little League shoulder), the wrist of gymnasts (gymnast wrist), and the knees of high-level athletes. This pattern of injury is unique to children, as the physes are two to five times weaker than the surrounding ligaments and capsular structures and therefore more prone to injury.

Then, we review the causes and appearances of stress-induced red marrow hyperplasia, which can mimic disease. Finally, common causes of marrow disease, including neoplastic marrow replacement and nonneoplastic edema-like marrow alterations, are discussed.

Normal Bone Marrow

Histologic Composition

The medullary space contains trabecular bone and bone marrow. The trabecular bone provides mineral storage and scaffolding. It has minimal signal intensity with MR imaging sequences due to lack of mobile protons. The bone marrow is composed of a combination of red (active, hematopoietic) and yellow (inactive, fatty) marrow. It supplies the basic functional units for oxygenation (red blood cells), cellular immunity (white blood cells), and coagulation (platelets).

The red marrow appears red due to the presence of hemoglobin. It represents the hematopoietic portion of the bone marrow, with roughly 60% hematopoietic cells and 40% adipocytes. Its fat fraction increases with age, from 40% in infants to 60% by age 70 years (1). Owing to its fat fraction, on T1-weighted images the red marrow is mildly hyperintense relative to skeletal muscle and intervertebral disks (2). The red marrow is also vascularized and therefore demonstrates mild gadolinium enhancement (3). This enhancement decreases with increasing age, correlating with the progressive conversion of red marrow to less vascular yellow marrow (4).

The yellow marrow appears yellow due to the carotenoids within the adipocytes. The function of yellow marrow is uncertain, and it is postulated to provide surface and/or nutritional support for the red marrow. It is composed of approximately 80% fat (1). Yellow marrow follows the MR signal intensity of subcutaneous fat and demonstrates no significant contrast enhancement (2).

MR Imaging Considerations

Although red marrow and yellow marrow are described as discrete elements for convenience, they are actually intermixed within the medullary space. Their proportions determine the overall distribution of fat and water (red marrow, 40% fat and 40% water; yellow marrow, 80% fat and 15% water), which ultimately determines the MR imaging signal intensity. Marrow disease often replaces the residential marrow fat with water. Therefore, the most useful sequences are the ones that can best display this difference between fat and water.

Because fat is the major component of both red and yellow marrow, the T1-weighted spin-echo sequence provides the most robust signal intensity (5), which provides optimal tissue contrast between yellow and red marrow as well as between yellow marrow and disease (6). On fluid-sensitive images, the signal intensity difference between red and yellow marrow is less apparent (yellow marrow has low signal intensity and red marrow has minimally high signal intensity relative to muscle). In contrast, most marrow diseases are hyperintense on fluid-sensitive images due to locally increased intracellular and extracellular water.

Contrast enhancement is less useful, as both normal red marrow and various diseases (infection, inflammation, and tumor) can enhance. The degree of normal marrow enhancement depends on the distribution and volume of red marrow. Therefore, in infants and young children with almost entirely hematopoietic marrow, contrast-enhanced images are even less sensitive in detection of subtle marrow disease.

The less routinely used MR imaging sequences include chemical shift imaging, diffusion-weighted imaging, and MR spectroscopy (7,8). Chemical shift imaging uses the difference in resonance frequency between fat and water photons to cancel their signal on out-of-phase images. Since fat is present in both red and yellow marrow but not in neoplastic lesions, these neoplastic lesions will not demonstrate the normal loss of signal on out-of-phase images. Signal drop of more than 20% has an odds ratio of 164 in predicting malignant pathologic vertebral body fractures (9). Preliminary data suggest that chemical shift imaging allows detection of replaced marrow in a background of abundant red marrow, which is particularly advantageous in evaluation of children (10).

Diffusion-weighted imaging is based on the Brownian motion of free water molecules in interstitial tissue. The calculated apparent diffusion coefficient (ADC) maps correlate inversely with tissue cellularity and cellular integrity, where lower ADC values reflect higher cellularity and allow detection of malignant lesions (11). A higher ADC value reflects areas of necrosis and can suggest a favorable response to cytotoxic therapy (12). However, preliminary studies in pediatric tumors suggest overlap in ADC values between benign and malignant lesions (13). In addition, diffusion-weighted imaging must be used with caution in infants and young children, as red marrow also restricts diffusion (14).

MR spectroscopy interrogates the metabolic profile of a lesion and is more commonly used in the brain. The relative paucity of literature on its use in the musculoskeletal system is due to signal dropout from cortical bone and spectral peak contamination from adipose tissue. Nevertheless, preliminary data suggest that an elevated choline signal may be used to discriminate malignant from benign lesions (15,16). The results from all three techniques—chemical shift imaging, diffusion-weighted imaging, and MR spectroscopy—are heavily based on adult studies. More studies are required to validate these results in children.

Less widely available imaging agents and protocols include ultrasmall superparamagnetic iron oxide (USPIO) particles and whole-body MR imaging. USPIO has the potential to distinguish between hypercellular red marrow and neoplastic marrow. Normal bone marrow contains macrophages, which phagocytose USPIO particles, and appears hyperintense on T2- and T2*-weighted images, while marrow replaced by neoplastic cells lacks these macrophages and appears hypointense (17). However, USPIO has not yet been approved for clinical use in the United States.

There is increased interest in use of whole-body MR imaging in recent years, mainly due

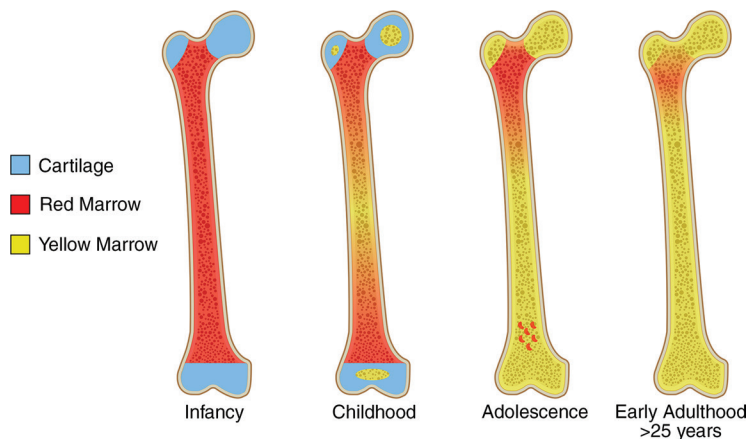
to advances in faster image acquisition and free-breathing protocols (18,19). The goal of whole-body MR imaging is maximum coverage of the body within the shortest possible imaging time. It typically uses the coronal imaging plane and T2-weighted fat-saturated sequences. The addition of diffusion-weighted imaging can be helpful in the setting of high-cellularity tumors, which restrict diffusion (20,21). In patients with multifocal disease, additional imaging planes and sequences with contrast material may be required. Whole-body MR imaging has been shown to be comparable to positron emission tomography/computed tomography (PET/CT) and better than bone scintigraphy in detection of neoplastic marrow, with sensitivities of 98%, 90%, and 30%, respectively (22). However, lack of a standardized protocol, possible long imaging time, and variable reimbursement are the main factors that hinder its more widespread use.

Red to Yellow Marrow Conversion

In the fetus, hematopoiesis begins in the yolk sac before transferring to the liver and spleen during the second trimester. As the medullary cavity forms within the developing long bones, hematopoiesis shifts into this space so that it is the primary site of red blood cell formation at term (4). Initially, the medullary cavity contains entirely red marrow with minimal fat; therefore, the marrow is isointense to muscle on T1-weighted images and hyperintense on fluid-sensitive images (23,24). During the postnatal period, the T1-weighted signal intensity rapidly increases, which reflects a progressive increase in the amount of marrow fat. In the perinatal period, the secondary ossification centers appear within the cartilaginous epiphyses and apophyses. They initially contain red marrow but are quickly replaced by yellow marrow within 6 months (25).

Red to yellow marrow conversion occurs throughout childhood and into early adulthood. An adult pattern is finally reached at approximately 25 years of age, characterized by the distribution of the red marrow limited to the axial skeleton (skull, vertebrae, ribs, sternum, and pelvis) and proximal aspects of the appendicular skeleton (femora and humeri) (2). This normal physiologic marrow conversion follows a predictable pattern throughout the body and within individual bones. Yellow marrow first appears peripherally in the terminal phalanges before birth and progresses centrally during the first 2 decades of life (26). Within long bones, such as the femora and humeri, this conversion starts in the epiphysis and apophysis, followed by the diaphysis, distal metaphysis, and finally proximal metaphysis (27,28) (Fig 1).

Figure 1. Red to yellow marrow conversion in the femur. At birth, the medullary cavity contains entirely hematopoietic red marrow. Secondary ossification centers appear within the perinatal period and quickly convert from red to yellow marrow within 6 months. Within the remainder of the bone, marrow conversion first starts in the diaphysis and progresses bidirectionally toward the metaphyses, faster distally than proximally, so that residual red marrow is mainly found only within the proximal metaphysis during adulthood.



Within the axial skeleton, the rate of marrow conversion is more gradual and continues into and throughout adulthood. The relative proportion of red marrow decreases by nearly half between the 1st and 8th decades, from 58% to 29% (29). From 0 to 4 months of age, the vertebral body ossification centers are dark on T1-weighted images when compared with the cartilage, due to the higher concentration of trabecular bone and hematopoietic marrow (30). By 6 months, the ossification centers become isointense relative to the cartilage. A T1-weighted bright mid horizontal band is often visible within these early ossification centers and corresponds to the sinusoidal blood space at the site of fusion between two contiguous somites (31).

Sebag et al (32) describe the vertebral marrow remaining predominantly iso- to hypointense to the disk before 1 year of age and hyperintense after 5 years of age, due to progressive red to yellow marrow conversion. However, this conversion may occur more rapidly (24). Marrow conversion often begins centrally around the basivertebral venous plexus, then extends peripherally toward the subchondral marrow adjacent to the endplates. It is normal to see persistent red marrow in the vertebral body with only isolated fatty marrow surrounding the basivertebral plexus as late as mid adulthood (33) (Fig 2). Although contrast enhancement of the basivertebral venous plexus persists throughout life, vertebral body enhancement is present only before 7 years of age due to its rich vascular supply, permeability of the capillaries, and the relative abundance of extravascular space (34).

In the pelvis, marrow signal intensity becomes heterogeneous during the 1st decade in the anterior ilium and acetabulum, due to non-uniform marrow conversion. This process continues into the 2nd decade in a heterogeneous but relatively symmetric fashion (35). During adulthood, residual red marrow is present in a

periarticular distribution, predominantly around the sacroiliac joints, followed by the hip joints and pubic symphysis (36).

Heterogeneous Red Marrow

Heterogeneous residual red marrow is a common finding in the pediatric population. Its stereotypical appearance and location help distinguish red marrow from pathologic marrow replacement. Areas of red marrow can be small and focal or large and geographic. Small islands of red marrow are common. A “bull’s-eye” appearance refers to a red marrow island with a central focus of yellow marrow, which is 95% sensitive and 99.5% specific for a benign process (37).

The larger geographic areas are typically within the femoral and humeral metaphyses. These large “flame-shaped” areas often abut the growth plate, extend into the metaphysis, and have sharply defined margins (38,39). Other common sites of red marrow include areas adjacent to the endplates of the vertebral bodies and the endosteum of the diaphyses of long bones. Occasionally, red marrow can be seen within the subchondral region of proximal epiphyses of the humeri and femora (40) (Fig 3).

Helpful features in distinguishing heterogeneous red marrow from a pathologic process include higher signal intensity relative to skeletal muscle on T1-weighted images, feathery margins representing red marrow elements interdigitating with the adjacent yellow marrow, relative bilaterality, and the absence of mass effect.

Red Marrow Hyperplasia

Red marrow may persist or proliferate in times of increased hematopoietic demand created by relative hypoxemic states, such as decreased oxygen-carrying capacity (chronic anemia, sickle cell disease, thalassemia), impaired oxygen delivery (smoking, high altitude, cyanotic congenital heart disease), and increased oxygen demand

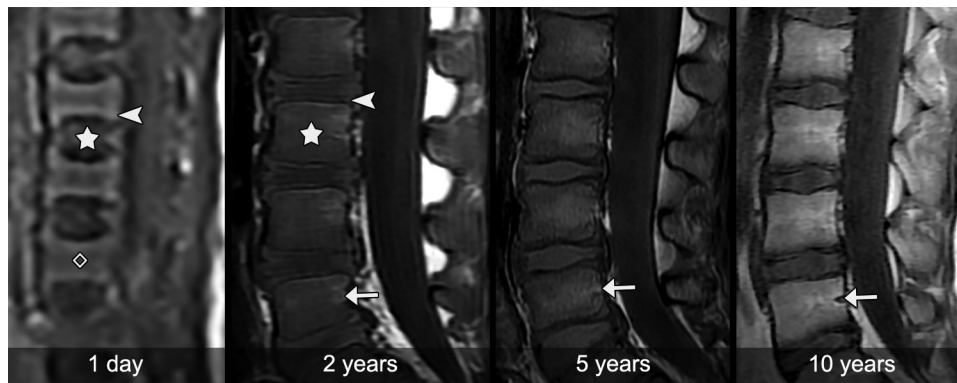


Figure 2. Vertebral body maturation and marrow conversion during early development. Sagittal T1-weighted images of the lumbar spine from 1 day of age to 10 years of age. At term, the vertebral body ossification centers (☆) are dark relative to the cartilaginous endplates (arrowhead) and disks (◇) due to the high concentration of trabecular bone and hematopoietic marrow. Note the more oval configuration of the ossification center and the bright mid horizontal band, which corresponds to the site of fusion between two contiguous somites. At 2 years of age, the ossification centers (☆) increase in size and the surrounding cartilage markedly thins (arrowhead). Vertebral body marrow conversion is a continuous process, which starts shortly after birth, first around the basivertebral venous plexus (arrow), then extends peripherally toward the subchondral marrow adjacent to the endplates. Typically, by 5 years of age, vertebral signal intensity is higher than in the adjacent disks.

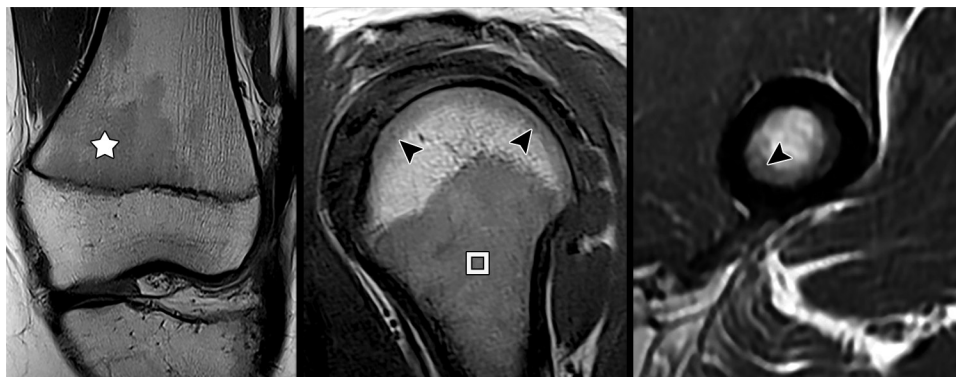


Figure 3. Normal heterogeneous red marrow. Left: T1-weighted image shows a large flame-shaped area of red marrow within the distal femoral metaphysis (☆). Center: T1-weighted image shows subchondral red marrow (arrowheads) within the proximal humeral epiphysis. There is diffuse red marrow hyperplasia within the proximal metaphysis (□) due to uncontrolled asthma. Right: T1-weighted image shows subendosteal red marrow within the mid shaft of the femur (arrowhead). Note that the red marrow is mildly hyperintense to muscle in all these examples.

(athletes). In severe cases, superimposed bone infarction can occur; in its acute phase, it is often indistinguishable from osteomyelitis based on imaging findings alone (41) (Fig 4).

During these times of systemic stress, the body shifts marrow distribution toward hematopoietic marrow (Fig 5). Yellow to red marrow reconversion occurs in the exact reverse order, centripetally from the axial to the appendicular skeleton and within the long bones, starting in the proximal metaphysis, followed by the distal metaphysis, and finally within the diaphysis (42). In times of severe stress, epiphyseal marrow reconversion, marrow cavity expansion, and/or extramedullary hematopoiesis can occur (43). Deviation from this pattern suggests an alternative diagnosis.

Nutritional disorders are another type of systemic stress that can induce nonspecific marrow changes. Scurvy is the result of vitamin C deficiency, which leads to impairment of the coagulation cascade. Case reports on the musculoskeletal manifestations of scurvy describe subperiosteal hemorrhage and nonspecific multifocal dark T1- and bright T2-weighted marrow changes (44) (Fig 6). Anorexia nervosa or severe cachexia causes hormonal alterations that can paradoxically lead to an increase in adipocytes within the medullary space, resulting in increased T1-weighted signal intensity (45). Rarely, serous atrophy occurs due to replacement of both yellow and red marrow with a gelatinous material, which is bright on both T1-weighted and fluid-sensitive images (46).



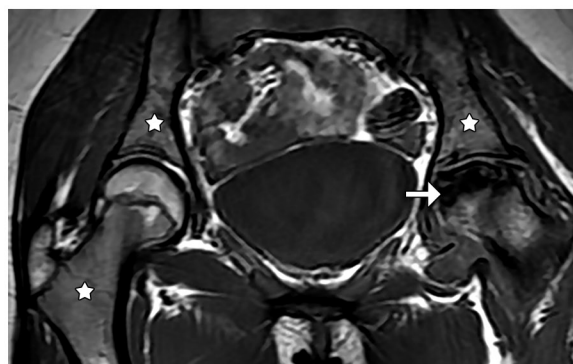
Figure 4. Bone infarctions due to sickle cell disease. (a–c) A 6-year-old boy presented during an acute veno-occlusive crisis. Sagittal T1-weighted (a), fluid-sensitive (b), and postcontrast (c) images of the humerus show heterogeneously enhancing medullary signal (□). This finding is nonspecific and mimics osteomyelitis. There is incomplete fat saturation of the proximal humerus (◇). (d) Coronal T1-weighted image of the pelvis in a 19-year-old man shows advanced avascular necrosis of the left femoral head with collapse (arrow). The mildly hyperintense signal within the right femoral metaphysis and pelvis (☆) is due to red marrow hyperplasia.

Neoplastic Replacement

Pediatric bone marrow tumors can arise from myeloid elements (leukemia and lymphoma), from mesenchymal elements (osteosarcoma, Ewing sarcoma), or represent hematogenous metastases. Tumors occur more commonly in the region of red marrow due to its richer vascularity and more active mitotic rates. In contrast to red marrow, which is mildly hyperintense relative to muscle on T1-weighted images, hypointensity relative to muscle has 81% accuracy for identifying an infiltrative process and hypointensity relative to intervertebral disks has 78% accuracy (47). Additional less sensitive and specific imaging clues include sharp transition between normal and abnormal marrow, mass effect, bone destruction, and an associated extraosseous soft-tissue mass.

Acute Leukemia

Acute leukemia is the most common pediatric malignancy (46), and acute lymphoblastic leukemia (ALL) is the most prevalent subtype. Three patterns of bone marrow replacement have been described: diffuse, patchy, and focal (4).



d.

The diffuse pattern is most common and occasionally can be overlooked during routine image interpretation, leading to delayed diagnosis. This pattern results in homogeneous loss of normal bright T1-weighted fatty marrow signal intensity with corresponding abnormally increased signal intensity on fluid-sensitive images, known as the “flip-flop” sign (Fig 7). However, this is a nonspecific pattern, which can also be seen with diffuse metastatic neuroblastoma and rhabdomyosarcoma (48). Although MR imaging is not part of either treatment or monitoring for acute leukemia, the abnormal marrow replacement can

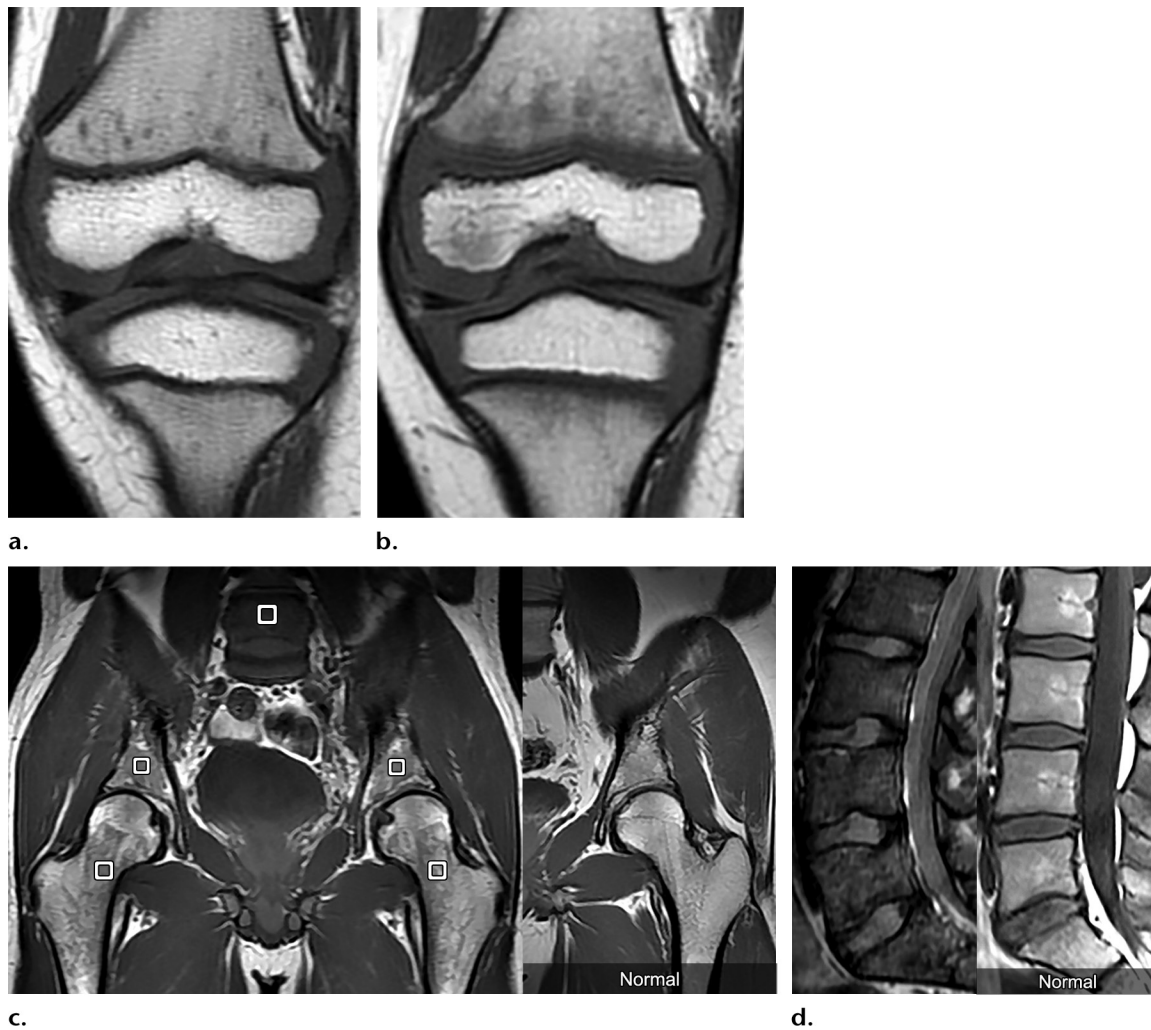


Figure 5. Red marrow hyperplasia. (a, b) A 3-year-old girl with aplastic anemia. Coronal T1-weighted images of the knee at initial presentation when the patient was transfusion-dependent (a) and during recovery (b) show expected stress-induced interval increase in the mildly hyperintense red marrow within the metaphyses. (c) A 23-year-old man with iron-deficiency anemia due to a bleeding gastric ulcer. Left: Coronal T1-weighted image of the pelvis shows heterogeneous increase in the volume of red marrow (□) within the spine, pelvis, and proximal femoral metaphyses. Right: Normal age- and gender-matched comparison. (d) A 20-year-old man with sickle cell disease. Left: Sagittal T1-weighted image of the lumbar spine shows diffuse heterogeneous low signal intensity of the vertebral bodies relative to the disk due to reconversion back to hematopoietic marrow. Multilevel central square endplate depressions are due to microvascular endplate occlusion and vertebral ischemia with subsequent relative overgrowth of the anterior and posterior corners, producing the characteristic “Lincoln log” or “H-shaped” vertebrae. Right: Normal age- and gender-matched comparison.

occasionally be detected in studies performed for other indications (Fig 8).

Bone infarction (avascular necrosis, osteonecrosis) or marrow necrosis is present in 6.5%–15% of patients with ALL, typically manifesting as nonspecific bone pain (49,50) (Fig 9). Imaging findings overlap between these two processes. Bone infarction is associated with impaired perfusion and typically occurs in the region of yellow marrow. Acutely, this results in marrow hemorrhage, edema, and liquefactive necrosis, which evolve into marrow fibrosis, trabecular disruption, and sclerosis. The classic “double-line” sign on fluid-sensitive images is apparent only during the subacute and chronic phases, consisting of an outer low-signal-intensity rim from sclerotic bone

and an inner higher-signal-intensity rim from inflammation and vascularized granulation tissue (51). Superimposed fracture and bone collapse during the advanced stages can lead to acute marrow edema (52).

In contrast, marrow necrosis is marrow infarction due to microvascular occlusion with preservation of the intervening trabecular bone. Although the exact mechanism is unknown, it is postulated that it may represent a combination of mechanical obstruction and inflammatory damage (53). This is best diagnosed on postcontrast images, where a geographic area of the marrow enhances peripherally but not centrally, which is similar to acute bone infarction. However, the evolution of the abnormality allows differentiation

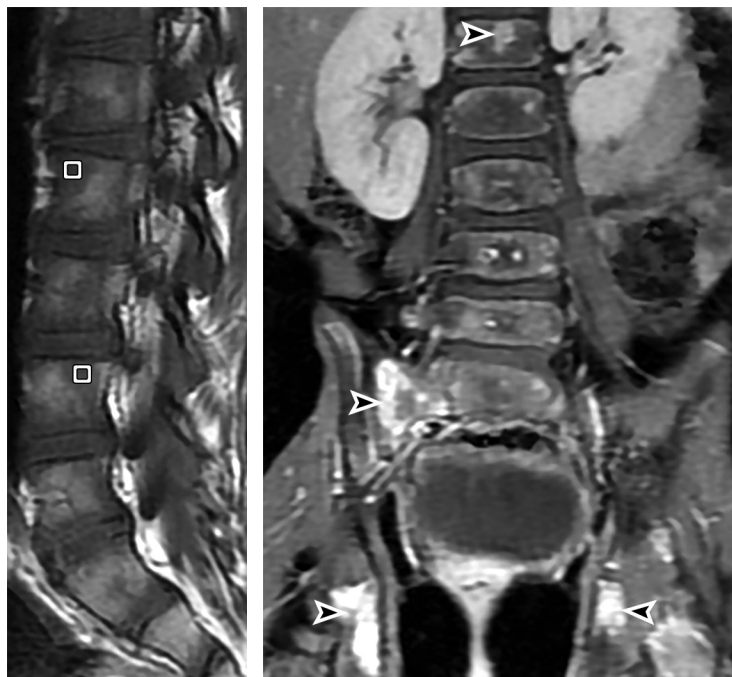


Figure 6. Scurvy in a 3-year-old autistic boy. (a) Parasagittal T1-weighted image of the lumbosacral spine shows multifocal patchy areas of isointense marrow signal (□) relative to the disk. (b) Coronal postcontrast fat-suppressed T1-weighted image shows enhancement of these vertebral areas as well as additional metaphyseal-equivalent areas within the pelvis (arrowheads). The patient's serum vitamin C level was less than 5 $\mu\text{mol/L}$ (normal, 23–114 $\mu\text{mol/L}$).

a.

b.

Figure 7. Diffuse marrow replacement due to ALL in an 8-year-old boy. Sagittal T1-weighted (a), fluid-sensitive (b), and postcontrast (c) images through the lumbar spine show diffuse homogeneous replacement of the normal fatty marrow with leukemic cells, resulting in low T1-weighted and high fluid-sensitive signal intensity, which is recognized as the flip-flop sign. Note the diffuse avid enhancement of the abnormal marrow and superimposed compression fractures (□ in a).



a.

b.

c.

between the two entities: necrotic marrow can heal and repopulate without progression to bone collapse (54). Although bone marrow necrosis is associated with malignancy in 80%–90% of cases, it is not specific to ALL and has been reported with neuroblastoma (55,56). Nonmalignant causes include infection, sickle cell disease, sepsis, and drug ingestion (55,57).

Lymphoma

Osseous involvement is more common with non-Hodgkin lymphoma than Hodgkin lymphoma

(25%–40% vs 5%–15%, respectively) and indicates advanced (stage IV) disease (59). Marrow replacement is often focal or patchy and less often diffuse, leading to high rates of false-negative bone marrow biopsies (Fig 10). Extrasosseous tumor extension can occur, often causing minimal or absent underlying cortical destruction due to its infiltrative nature.

Primary Osseous Sarcomas

The most common primary malignant bone tumors of children and young adults are osteo-

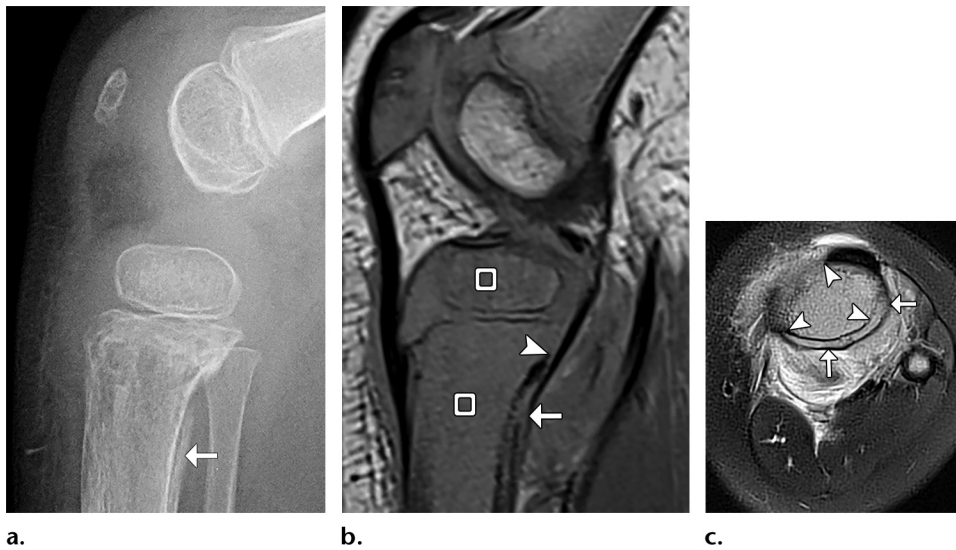


Figure 8. Pathologic fracture due to ALL in a 2-year-old girl. (a) Lateral knee radiograph shows a pathologic fracture through an aggressive lytic lesion in the proximal tibial metaphysis. Note the posterior periosteal elevation (arrow). (b, c) Sagittal T1-weighted image of the knee (b) and axial post-contrast image through the tibial metaphysis (c) show a diffuse marrow replacement process within the proximal tibia (□ in b) with cortical breakthrough (arrowheads) and periosteal elevation (arrows). The surrounding soft-tissue enhancement represents a combination of fracture-induced inflammation and neoplastic infiltration.

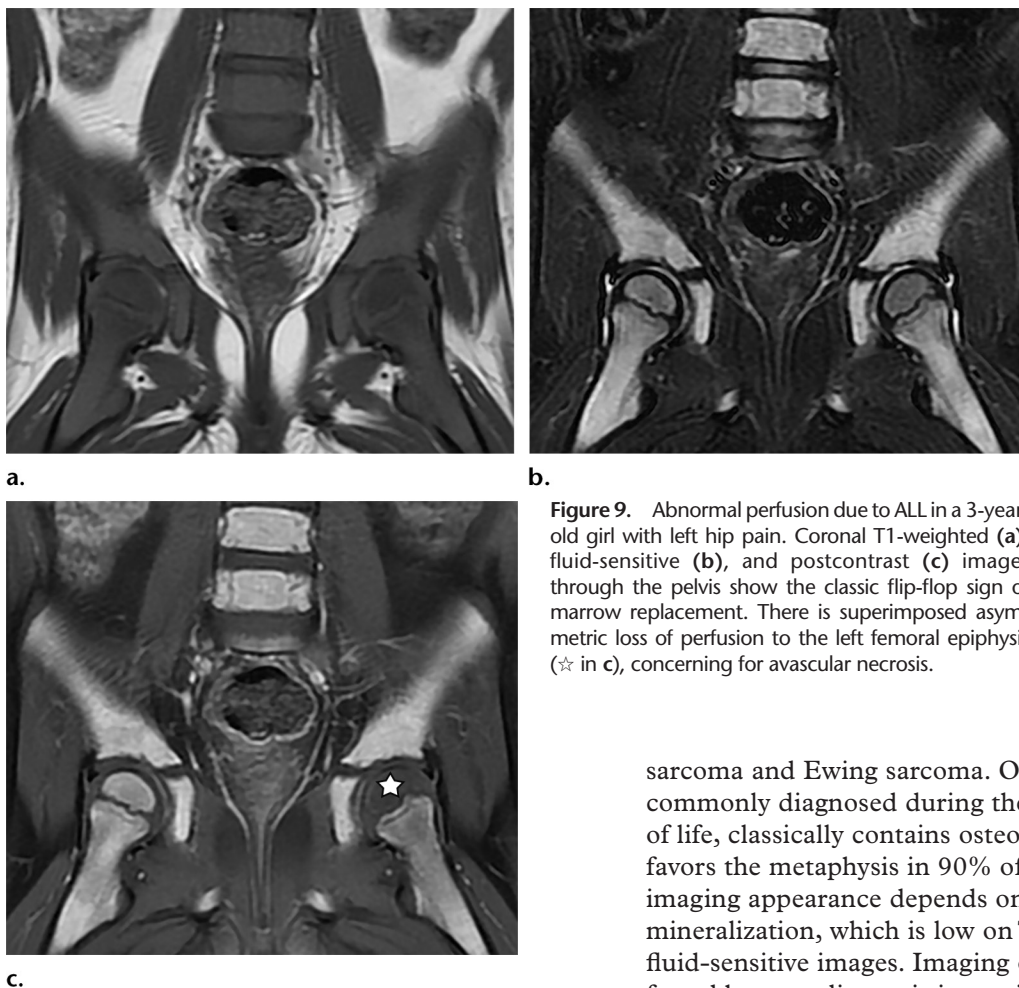


Figure 9. Abnormal perfusion due to ALL in a 3-year-old girl with left hip pain. Coronal T1-weighted (a), fluid-sensitive (b), and postcontrast (c) images through the pelvis show the classic flip-flop sign of marrow replacement. There is superimposed asymmetric loss of perfusion to the left femoral epiphysis (☆ in c), concerning for avascular necrosis.

sarcoma and Ewing sarcoma. Osteosarcoma, commonly diagnosed during the 2nd decade of life, classically contains osteoid matrix and favors the metaphysis in 90% of cases. Its MR imaging appearance depends on the degree of mineralization, which is low on T1-weighted and fluid-sensitive images. Imaging of the entire affected bone at diagnosis is crucial for detection of skip lesions and subsequent surgical planning. Micrometastatic disease is presumed present at



Figure 10. Hodgkin lymphoma in a 9-year-old boy. Sagittal T1-weighted (**a**) and fluid-sensitive (**b**) images of the thoracic spine show minimally heterogeneous, global replacement of the normal fatty marrow with lymphoma cells. Note the extraosseous soft-tissue mass in the spinal canal (○) with focal mass effect on the proximal thoracic cord and the relatively intact adjacent vertebral cortices. (**c**) T1-weighted image showing a normal age- and gender-matched comparison.

the time of diagnosis, which necessitates neoadjuvant chemotherapy.

Ewing sarcoma affects a younger age group but is rare under the age of 5 years. It favors the diaphysis, often with a large associated extraosseous soft-tissue mass (Fig 11). Ewing sarcoma is extremely radiosensitive; for cases of unresectable disease, radiation therapy is often used for local control.

Hematogenous Metastases

In the pediatric population, metastatic disease is most often secondary to neuroblastoma, followed by primary bone or soft-tissue sarcomas (ie, Ewing sarcoma and rhabdomyosarcoma). Since the spread of hematogenous metastases is dependent on blood flow, sites of red marrow are more frequently involved due to their increased vascularity (4,60). Metastases are commonly multifocal, although neuroblastoma and rhabdomyosarcoma can appear diffuse and mimic leukemia (48) (Fig 12).

On fluid-sensitive images, the “halo sign” is characterized by a peripheral rim of hyperintensity, which is hypothesized to represent focal trabecular destruction and replacement with fluid. This sign is 75% sensitive and 99.5% specific for metastases (37). Overall, MR imaging allows detection of more metastases than skeletal scintigraphy,

as it does not rely on cortical involvement (22,61).

Treatment-related Changes

Radiation, chemotherapy, granulocyte colony-stimulating factor, and bone marrow transplant are routinely used in treatment of neoplasms and lead to temporary or permanent changes in marrow composition and MR imaging signal intensity. Understanding the expected posttreatment changes is crucial for identifying residual or recurrent neoplastic marrow involvement.

Radiation therapy is often limited to the region of disease, with the goal of establishing local disease control (Fig 12). During the first 2 weeks after irradiation, bone marrow may show no change, edema, or hemorrhage, leading to a variable imaging appearance (62). A mild transient increase in contrast enhancement may be seen due to increased vascular permeability. After 3–6 weeks, there is preferential disappearance of the red marrow, leading to heterogeneously increased signal intensity on T1-weighted images. After 6 weeks, the fatty marrow transformation becomes more homogeneous (63) (Fig 13).

Recovery of normal marrow signal intensity is largely dependent on the patient’s age and the radiation dose. Younger patients and patients

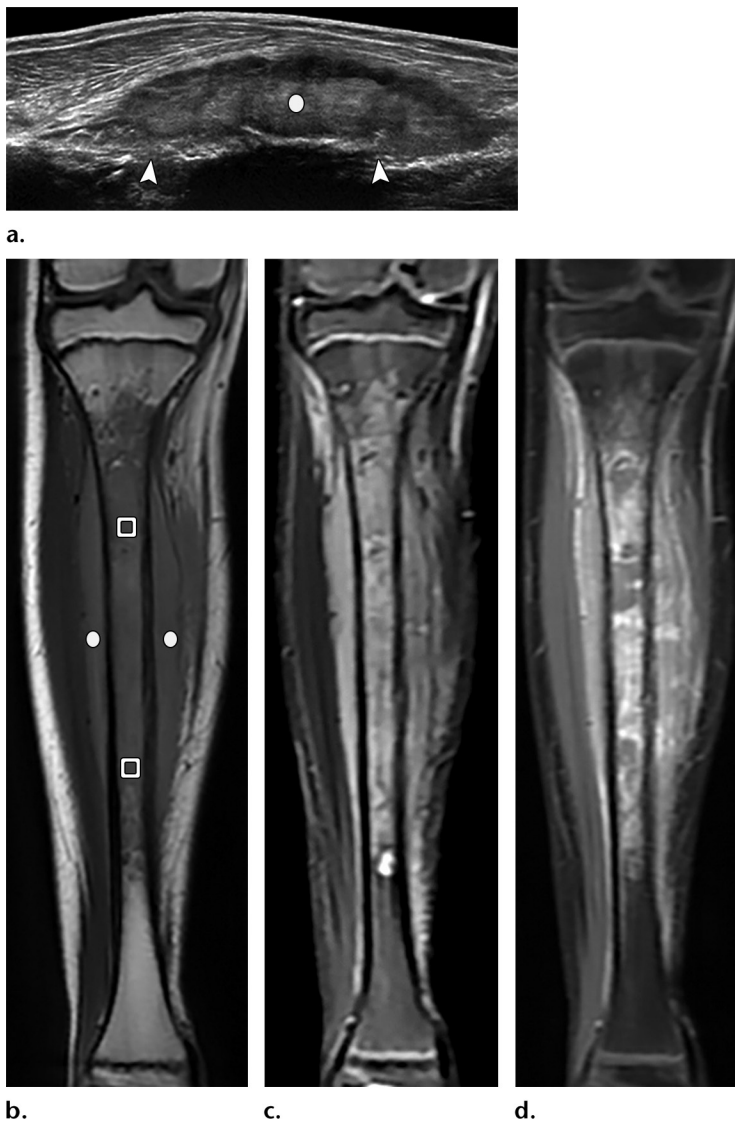


Figure 11. Ewing sarcoma in an 11-year-old boy. (a) Longitudinal gray-scale ultrasonographic image of the calf shows a heterogeneous mass (O) with underlying cortical irregularity (arrowheads). (b–d) Coronal T1-weighted (b), fluid-sensitive (c), and postcontrast (d) images show an aggressive, heterogeneously enhancing lesion with extensive tibial marrow replacement (□ in b). Note the associated circumferential soft-tissue mass (O in b).

receiving less than 30–40 Gy are more likely to recover with full marrow regeneration. At doses greater than 40–50 Gy, little to no regeneration occurs due to sinusoidal destruction (64).

Early signs of marrow regeneration include either a diffuse mottled appearance or a peripheral band of mildly increased T1-weighted signal intensity relative to muscle, reflecting hematopoietic marrow (65). Marrow changes are classically restricted to the region covered by the radiation port, but altered marrow signal intensity can occur in adjacent structures due to a combination of indirect effects and/or scattered radiation (66,67). Complications after radiation therapy include growth disturbance in the skeletally immature, osteonecrosis, insufficiency fractures, and secondary radiation-induced benign and malignant neoplasms, most commonly osteochondroma and osteosarcoma (68,69).

Chemotherapy changes are often diffuse. During the 1st week, the marrow is character-

ized by edema secondary to dilatation and hyperpermeability of the sinusoids. In the following weeks, the cytotoxic effect decreases the number of myeloid precursors, leading to fatty marrow transformation. Within 3–4 weeks, red marrow regeneration begins, typically in a multifocal pattern with numerous small foci of red marrow (70). After successful chemotherapy, the marrow appearance may or may not completely normalize. Complications of chemotherapy include methotrexate-induced osteopathy (osteopenia, insufficiency fractures, multifocal involvement) (71,72), hypophosphatemic rickets from ifosfamide-induced nephrotoxicity, isotretinoin-induced cortical hyperostoses, and bone infarction (73).

Granulocyte colony-stimulating factor is often administered in conjunction with chemotherapy to stimulate myeloid cell production and limit aplasia. Stimulation of red marrow proliferation typically occurs in a diffuse, patchy pattern and

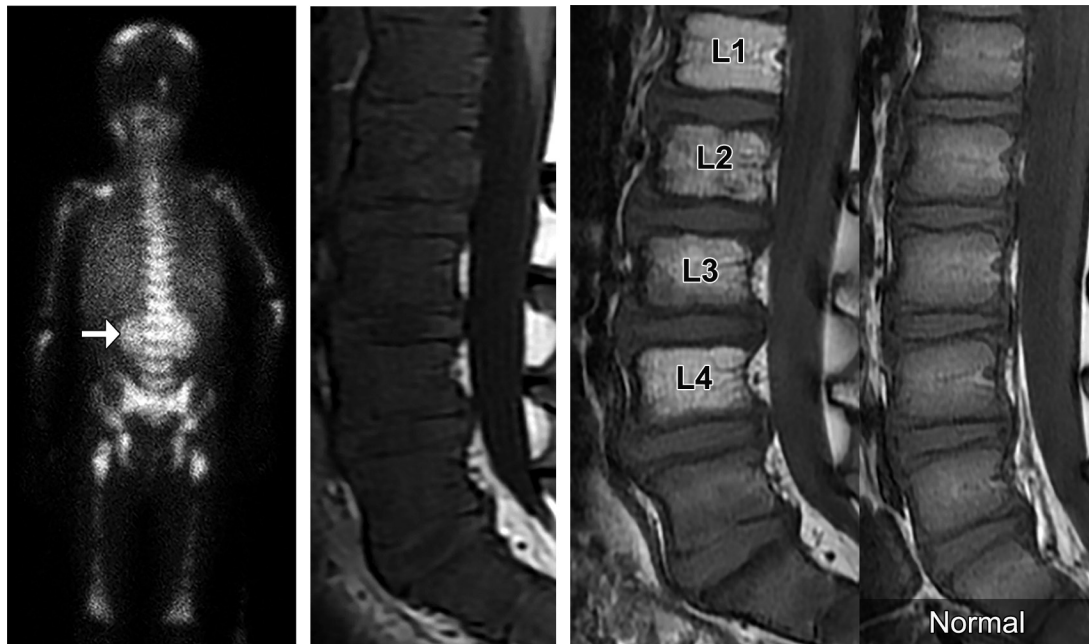
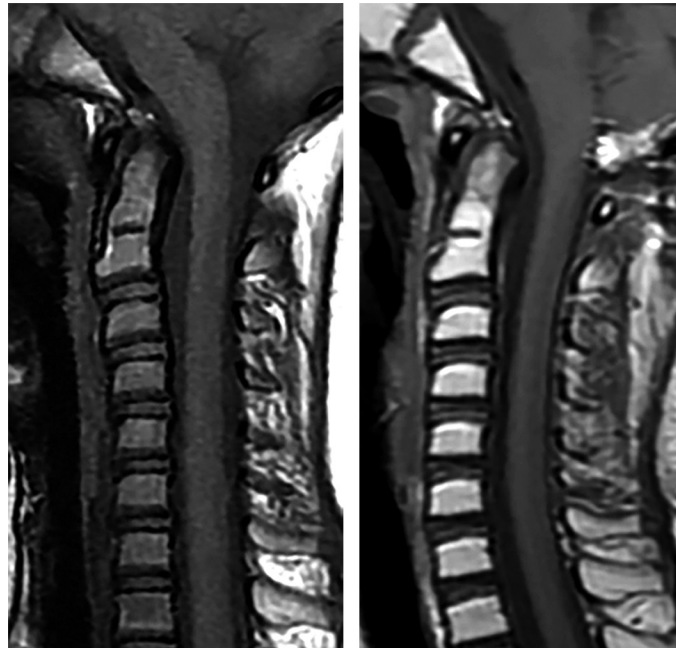


Figure 12. Diffuse metastatic neuroblastoma in a 4-year-old boy. (a) Posterior projection iodine 131 metaiodobenzylguanidine scan shows the midabdominal primary tumor (arrow) and extensive metastases throughout the axial and proximal appendicular skeleton. (b) Sagittal T1-weighted image of the lumbosacral spine before treatment shows diffuse fatty marrow replacement by neuroblastoma with the vertebral bodies isointense to the disks. (c) Left: Post-radiation therapy image shows fatty marrow conversion of the vertebrae within the radiation field (L1–L4). Right: Normal age- and gender-matched comparison.

Figure 13. Metastatic medulloblastoma treated with radiation therapy in a 6-year-old girl. Sagittal T1-weighted images of the craniocervical junction before (a) and 6 months after (b) radiation therapy show radiation-induced diffuse homogeneous fatty marrow conversion.



a.

b.

can mimic disease (74). The effect occurs rapidly, maximizes at 2 weeks, and normalizes 6 weeks after discontinuation of the growth factor (74).

Bone marrow transplant involves ablation of the patient's native marrow and infusion of either autologous or allogenic stem cells to reconstitute

a new marrow free of neoplastic cells. Two to 4 weeks after stem cell infusion, a peripheral band-like pattern of mildly increased T1-weighted signal intensity relative to muscle appears, which reflects regenerating hematopoietic cells repopulating along the subendosteal sinusoids. In

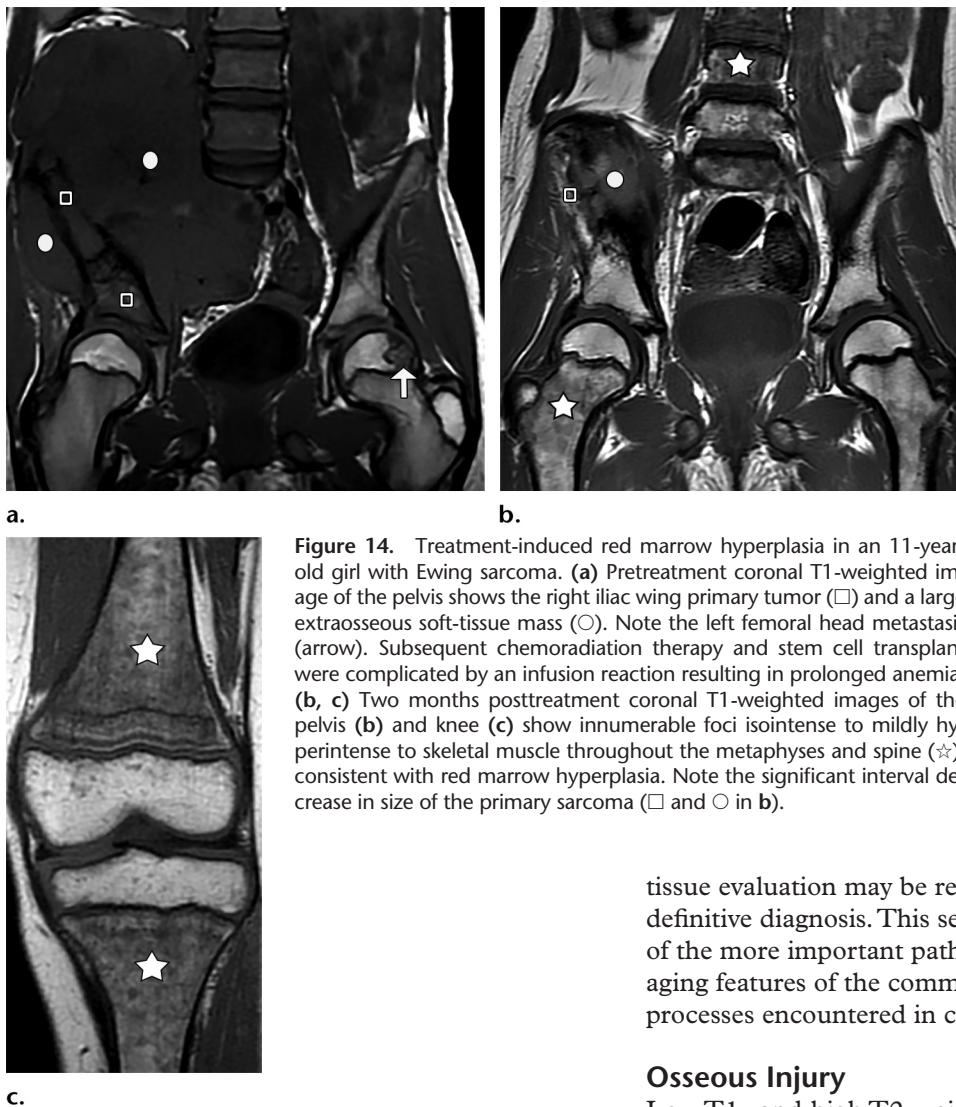


Figure 14. Treatment-induced red marrow hyperplasia in an 11-year-old girl with Ewing sarcoma. **(a)** Pretreatment coronal T1-weighted image of the pelvis shows the right iliac wing primary tumor (□) and a large extraosseous soft-tissue mass (○). Note the left femoral head metastasis (arrow). Subsequent chemoradiation therapy and stem cell transplant were complicated by an infusion reaction resulting in prolonged anemia. **(b, c)** Two months posttreatment coronal T1-weighted images of the pelvis **(b)** and knee **(c)** show innumerable foci isointense to mildly hyperintense to skeletal muscle throughout the metaphyses and spine (☆), consistent with red marrow hyperplasia. Note the significant interval decrease in size of the primary sarcoma (□ and ○ in **b**).

other areas, a multifocal pattern with numerous small foci of red marrow can be present (Fig 14). Posttransplant changes typically stabilize by 3 months. In patients with successfully reconstituted marrow, T1-weighted signal intensity often remains increased compared with that of age-matched controls (75).

Nonneoplastic Infiltration

A diverse group of nonmalignant processes can produce low T1-weighted and high fluid-sensitive signal intensity within the marrow, including trauma, infection, inflammation, altered biomechanics, and chronic regional pain syndrome. Although this imaging pattern is loosely termed *bone marrow edema*, histopathologic examination demonstrates a variable amount of hemorrhage, fibrosis, and/or necrosis in addition to fluid; therefore, it is better termed *edema-like lesion* (76). As imaging findings often overlap, the clinical history, laboratory assessment, and potentially

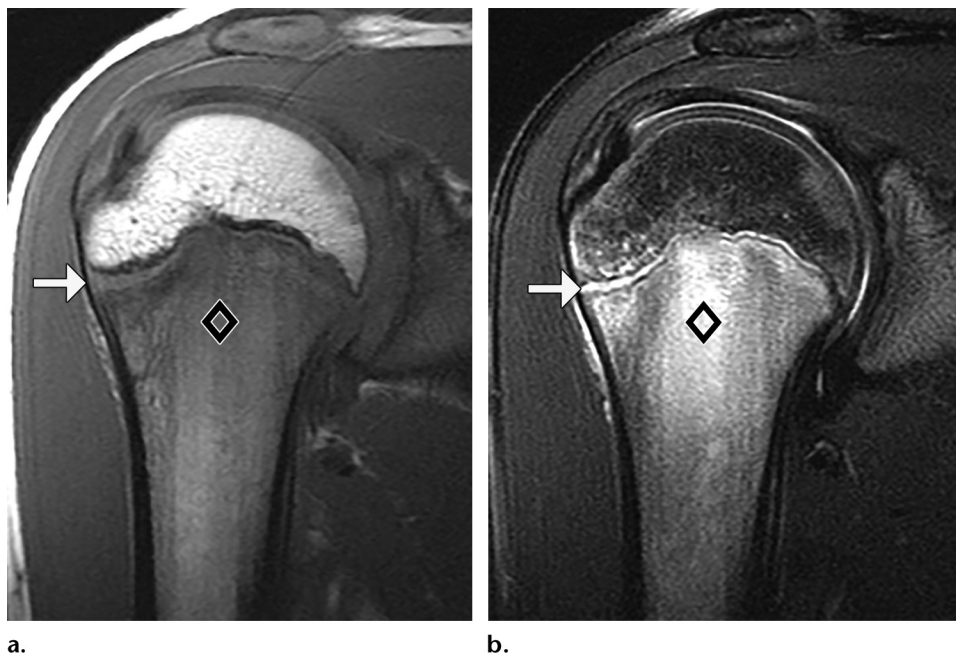
tissue evaluation may be required to establish the definitive diagnosis. This section highlights some of the more important pathophysiologic and imaging features of the common edema-like marrow processes encountered in children.

Osseous Injury

Low T1- and high T2-weighted signal intensity at the site of osseous injury reflects a combination of edema and hemorrhage. The spectrum of injury ranges from fracture and bone contusion to chronic microtrauma from overuse. In skeletally immature patients, 18% of fractures involve the physis. There is a subsequent risk of growth arrest, which is most common in the distal femur and tibia, accounting for 35% and 30% of cases, respectively (77,78). A bone contusion (also known as a bone bruise) is the result of low-impact trauma to the cancellous bone leading to trabecular microfracture. In athletes, asymptomatic bone marrow edema is often present (79), which is thought to represent a combination of contusion (80) and stress-induced hyperperfusion leading to bone remodeling (81).

Overuse injuries include both stress fractures and physeal injuries. The most common sites for stress fractures in children are the tibia, fibula, and pars interarticularis (78). Repetitive strenuous activity can cause microtrauma to the physis due to disruption of the metaphyseal vascular

Figure 15. Little League shoulder in a 14-year-old male baseball pitcher. Oblique coronal T1-weighted (a) and fluid-sensitive (b) images of the right shoulder show subtle asymmetric peripheral physeal widening (arrow), with dark T1-weighted and bright fluid-sensitive reactive signal intensity in the adjacent metaphysis (◇).



supply, resulting in extension of hypertrophic chondrocytes into the metaphysis. This is most common in the shoulder of pitchers (Little League shoulder) (82), the wrist of gymnasts (gymnast wrist) (83), and the knees of high-level athletes (84) (Fig 15). This pattern of injury is unique to children, as the physes are two to five times weaker than the surrounding ligaments and capsular structures and therefore more prone to injury (85). The resulting physeal widening and irregularity can progress to transphyseal bony bridging (78,84).

In adolescents, focal periphyseal edema can be present along the central portion of a closing physis and extend into both the metaphysis and epiphysis. This is postulated to represent focal stress and microtrauma due to decreased flexibility at this initial site of normal physiologic physeal closure (86).

Osteomyelitis

Osteomyelitis has a prevalence of two to 13 per 100 000 children in developed countries, and 40% of cases occur in preschool children. The most common sites of infection are the femur, followed by the pelvis, tibia, and humerus (87). *Staphylococcus aureus* is the most common pathogen (Fig 16). In more recent years, *Kingella kingae* has become the leading Gram-negative organism among children under 4 years of age and manifests as a more indolent infection (88).

Acute osteomyelitis is often secondary to hematogenous spread. Metaphyseal seeding is common due to sluggish flow within the meta-

physeal venules. In infants under 18 months of age, transphyseal vessels permit epiphyseal involvement. Infectious exudate can decompress into the subperiosteal space (subperiosteal abscess) or surrounding structures (pyomyositis and septic arthritis) and/or elicit local inflammatory reaction and deep venous thrombosis (89).

Radiographs are insensitive in the first 2 weeks. MR imaging is the comprehensive imaging modality of choice, which allows assessment of both the bone marrow and surrounding soft tissues. The abnormal marrow signal intensity (low on T1-weighted images and high on fluid-sensitive images) arises from a combination of infiltrated inflammatory cells and reactive inflammatory response (Fig 16). Imaging findings that favor infection over neoplasm include poorly defined transition between normal and abnormal marrow, intramedullary fat lobules, and extraosseous fat-fluid level. The latter two are due to necrosis of medullary lipocytes (90). If the marrow is normal on precontrast images, additional gadolinium-enhanced images add no additional value (91). Exceptions to this rule include suspected epiphyseal cartilage infection and epidural abscess (90,92).

Chronic osteomyelitis is defined by persistent infection after 1 month of treatment. This may manifest as a small focus of disease such as a Brodie abscess, more pervasive disease with sequestrum and involucrum, or uniformly dense sclerosis. In contrast to acute osteomyelitis, chronic osteomyelitis has a better-defined interface between normal and diseased marrow (93) (Fig 17).

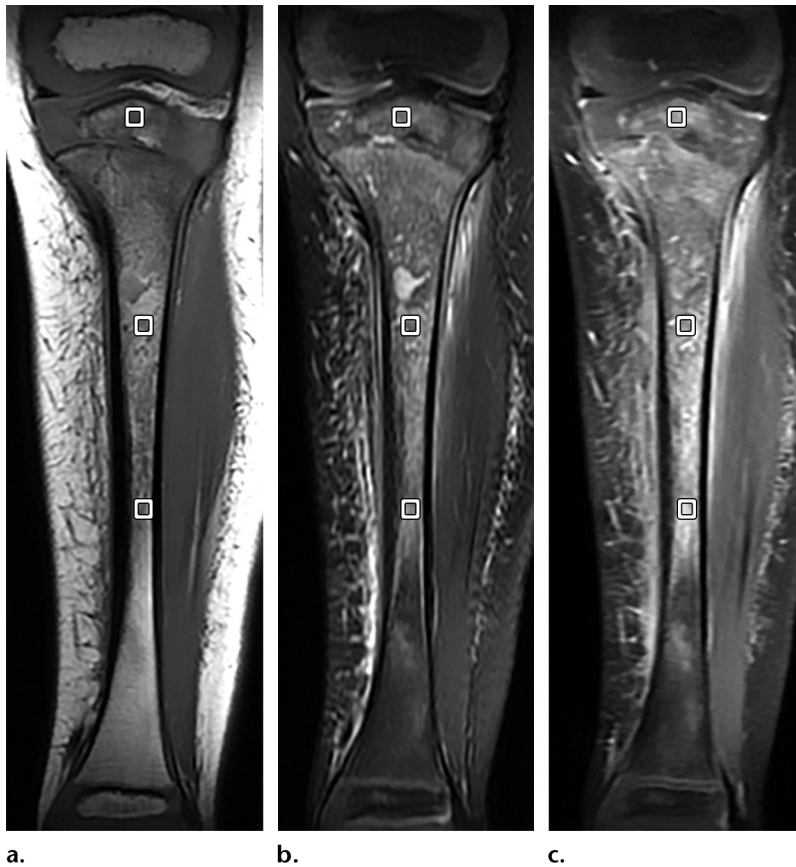


Figure 16. Acute *S aureus* osteomyelitis in a 3-year-old girl. Coronal T1-weighted (a), fluid-sensitive (b), and postcontrast (c) images show heterogeneously enhancing tibial intramedullary inflammatory changes (□) and extensive surrounding soft-tissue inflammation.

Chronic Recurrent Multifocal Osteomyelitis

Chronic recurrent multifocal osteomyelitis (CRMO) is postulated to represent an autoinflammatory process. It is a diagnosis of exclusion, reliant on a combination of factors including prolonged and/or recurrent clinical course, typical imaging appearance, laboratory findings that mimic osteomyelitis (but without a causative organism), no response to antibiotics, and positive response to nonsteroidal anti-inflammatory drugs (NSAIDs). Primary differential diagnoses include acute bacterial osteomyelitis, metastases, and Langerhans cell histiocytosis (94).

CRMO commonly involves the metaphyses of long bones and the pelvis, spine, and medial clavicle. The metaphyseal lesions are more common in the lower extremities and juxtaphyseal in location, with widely variable radiographic appearances ranging from normal to lytic, sclerotic, or mixed (94,95) (Fig 18). Bilateral, symmetric, synchronous involvement is insensitive but specific for CRMO (95). Medial clavicle involvement is characterized by significant hyperostosis and lack of extension to the sternoclavicular joint (94). Spine involvement is often multifocal and vertebral plana can occur, which mimics Langerhans cell histiocytosis or metastatic disease (lymphoma, leukemia, and neuroblastoma).

With the exception of the spine, MR imaging is highly sensitive in detection of active disease, which appears as bone marrow edema and contrast enhancement, while quiescent sites appear dark on both T1- and T2-weighted images due to sclerosis (96). Given the often multifocal nature of the disease, whole-body imaging helps identify additional asymptomatic lesions. Although whole-body imaging has traditionally been performed with skeletal survey or technetium 99m bone scintigraphy, there is increased use of whole-body MR imaging given its advantage of avoiding radiation (94).

Complications can include growth disturbances secondary to premature physal closure and cord compression or kyphoscoliosis from spinal involvement. Although most cases spontaneously resolve, some can last up to 25 years (97).

Juvenile Inflammatory Arthritis

Juvenile inflammatory arthritis (JIA) is a heterogeneous group of arthritides with onset before 16 years of age and symptoms persisting for over 6 weeks. The most common sites of involvement are the knee, followed by the ankle, wrist, hand, elbow, and hip (98). Seven distinct subtypes are recognized by the International League of Associations for Rheumatology, and all involve chronic inflammation of the synovium and

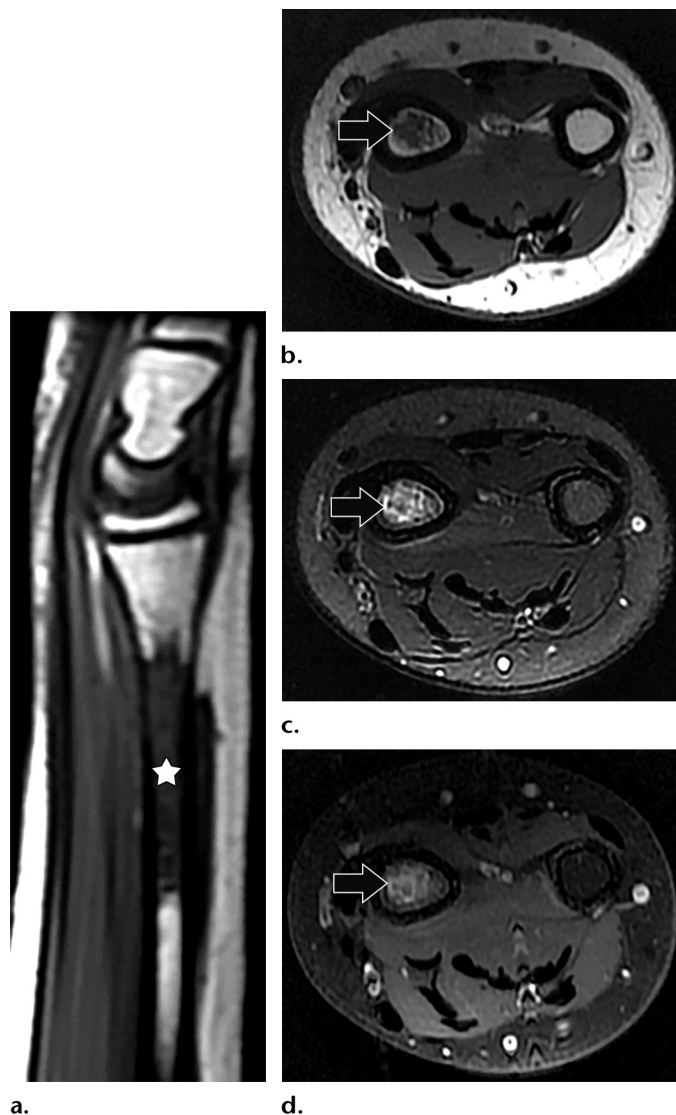


Figure 17. Chronic osteomyelitis in a 10-year-old girl. (a) Sagittal T1-weighted image of the distal radius shows a well-demarcated area of marrow replacement (☆). (b–d) Axial T1-weighted (b), fluid-sensitive (c), and postcontrast (d) images show the marrow replacement (arrow), which is bright on the fluid-sensitive image and demonstrates mild enhancement, compared with the normal marrow in the adjacent ulna. Targeted biopsy revealed chronic inflammation.

periarticular tissues. In contrast to the adult pattern of periarticular destruction in rheumatoid arthritis, inflammation in JIA begins at the surface of the epiphyseal cartilage and spreads to the underlying ossification center, leading to skeletal undergrowth or overgrowth and joint malalignment. Joint space narrowing develops early with progression to erosions and ankylosis (99).

MR imaging is not routinely used in diagnosis of JIA. However, in ambiguous cases or when it involves deep or complex joints, MR imaging remains the most comprehensive imaging modality, as it can simultaneously exclude alternative diagnoses and assess for the presence of osteoarticular inflammation.

Altered Biomechanics

Nonspecific marrow change from immobilization is often encountered in routine practice and is reproducible in experimental settings. For example, temporary overpronation of the lateral foot for 2

weeks induced multifocal marrow edema in 92% of volunteers (100). These often asymptomatic, patchy areas of marrow edema favor the hindfoot and are often subcortical, subchondral, and subenthelial in location (101). These findings may represent disuse osteopenia and/or microfractures in the setting of decreased bone integrity (Fig 19). However, bilateral, symmetric, patchy to confluent marrow changes are also seen in the feet of asymptomatic active children (102,103), postulated to represent residual red marrow or physiologic stress from increased bone remodeling, as they are absent in children after 15 years of age (103). Therefore, the clinical history and the patient's symptoms are invaluable during image interpretation.

Bone Marrow Edema Syndromes

Bone marrow edema syndromes include transient osteoporosis of the hip (TOH), regional migratory osteoporosis (RMO), and chronic regional

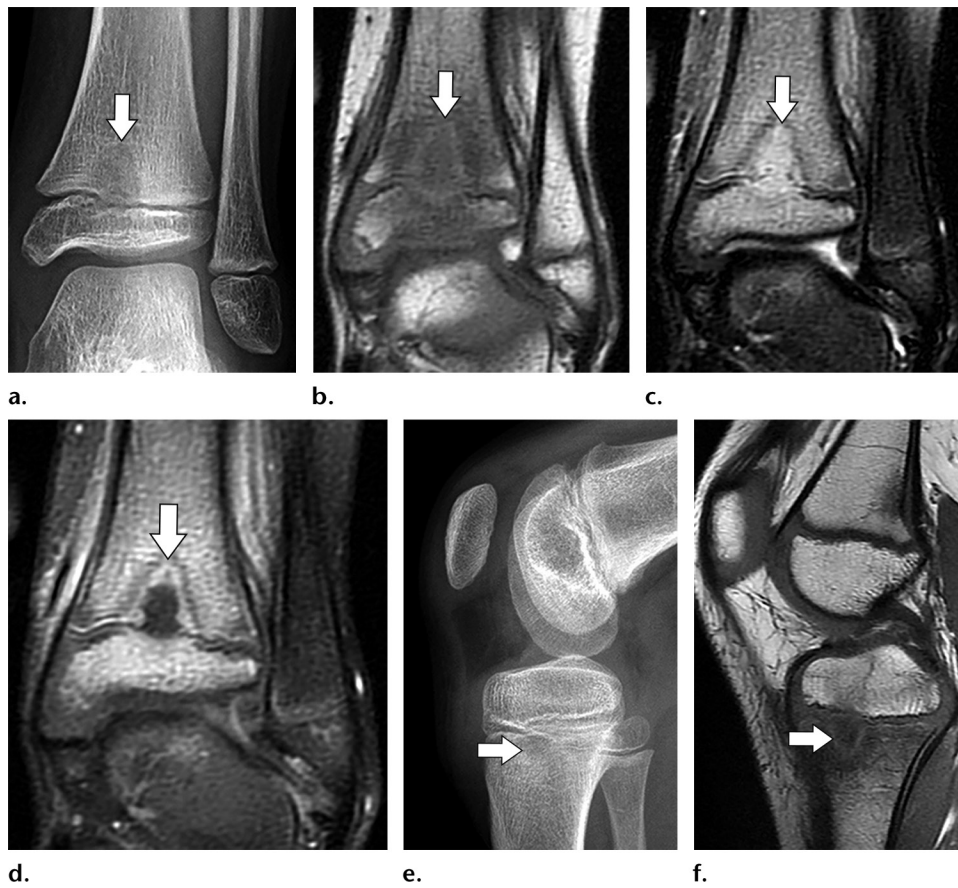


Figure 18. CRMO in a 7-year-old girl. Anteroposterior ankle radiograph (a) and coronal T1-weighted (b), fluid-sensitive (c), and postcontrast (d) images show a distal tibial metaphyseal lytic lesion with peripheral enhancement and a hypointense sclerotic rim (arrow). Note the transphyseal extension into the epiphysis and surrounding reactive marrow changes. (e, f) Lateral knee radiograph (e) and sagittal T1-weighted image (f) of the contralateral knee show a similar metaphyseal lesion (arrow). Bone biopsy excluded infection, and the patient improved with anti-inflammatory medication.

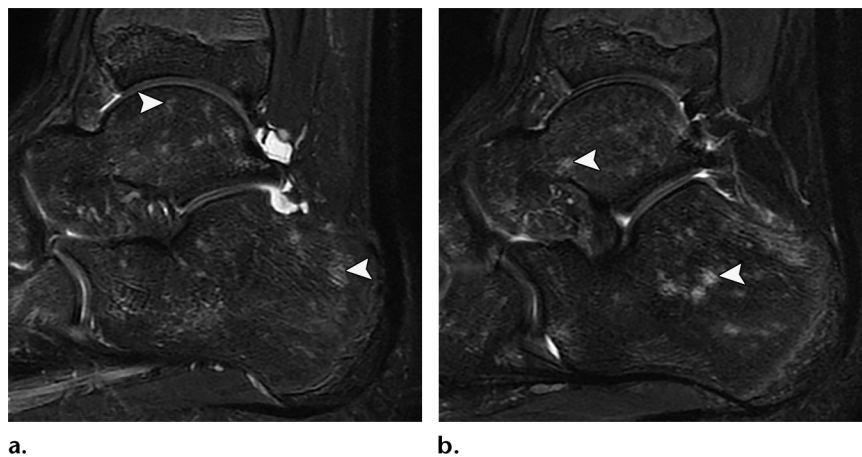


Figure 19. Nonspecific hindfoot patchy marrow signal intensity in a 12-year-old boy 1 year after a right ankle sprain. He presented with bilateral diffuse ankle pain with sports activity but not with daily activity. Sagittal fluid-sensitive images of the right (a) and left (b) hindfoot show bilateral scattered foci of hyperintensity in the talus and calcaneus (arrowheads). This imaging finding is nonspecific, with the most common causes being immobilization, residual red marrow, or physiologic stress. The patient improved with physical therapy.

pain syndrome (CRPS). TOH and RMO are more common in adults and rare in children (104). Therefore, the remainder of this discussion will be limited to CRPS.

CRPS affects children 5–17 years of age but has a predilection for adolescent girls (105). Fracture is the most common inciting event,

accounting for up to 40% of cases, followed by blunt trauma and surgery (Fig 20). The pathophysiology is hypothesized to be secondary to an increased inflammatory or immune response, leading to sensitization of nociceptive receptors and subsequent hyperalgesia (106). Sympathetic dysfunction results in abnormal vasomotor and

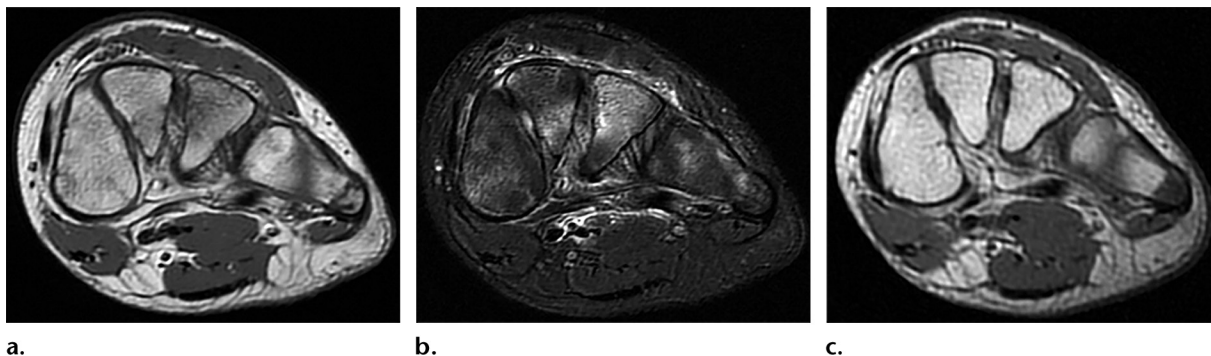


Figure 20. CRPS in an 11-year-old girl with persistent pain, temperature change, and hypersensitivity after blunt trauma. (a, b) Short-axis T1-weighted (a) and fluid-sensitive (b) images through the distal midfoot show heterogeneous marrow signal intensity and surrounding deep soft-tissue edema. These imaging findings are nonspecific and are indistinguishable from changes due to altered biomechanics. (c) T1-weighted image immediately after the initial trauma 3 months earlier shows normal homogeneous fatty marrow signal intensity.

sudomotor function, which includes skin discoloration, hyperhidrosis, temperature changes, and edema. In the late stages, loss of function and muscle contractures occur (107).

Within 2–8 weeks, patchy subchondral or subperiosteal osteopenia can be radiographically visible, which progresses to severe diffuse periarticular osteopenia (107). Unlike in adults, where upper extremity involvement is more common, the lower extremity is five times more likely to be affected in children. In the acute setting, MR imaging demonstrates extensive patchy and subcortical marrow edema with occasional articular erosions. Extrasosseous manifestations include skin thickening, periarticular soft-tissue edema, muscle atrophy, and joint effusion (Fig 20). In some cases, the abnormal findings may be limited only to the soft tissues (106).

In the chronic stages, there is periarticular soft-tissue atrophy. The imaging appearance is nonspecific and often overlaps with those of altered biomechanics and disuse. Treatment is complex, with a favorable outcome seen in 1%–43% of patients (105).

Conclusion

The bone marrow is a dynamic organ, and its composition changes throughout life in response to normal maturation (red to yellow conversion) and stress (yellow to red reconversion). Any deviation from the predictable pattern of conversion and reconversion can suggest underlying disease and should be investigated. Since MR imaging is increasingly used in imaging of pediatric patients and the bone marrow is visible in every MR imaging study, the radiologist may be the first to detect unsuspected marrow disease, triggering further evaluation and changes in patient management. MR imaging is highly sensitive in detection of altered marrow signal intensity, which can represent benign (heteroge-

neous red marrow and red marrow hyperplasia) or pathologic (neoplastic replacement and non-neoplastic edema-like infiltration) processes. As imaging findings in vastly different diseases often overlap, a definitive diagnosis is often reliant on a combination of imaging findings, clinical evaluation, laboratory assessment, and occasionally tissue analysis.

References

- Steiner RM, Mitchell DG, Rao VM, Schweitzer ME. Magnetic resonance imaging of diffuse bone marrow disease. *Radiol Clin North Am* 1993;31(2):383–409.
- Vande Berg BC, Malghem J, Lecouvet FE, Maldague B. Magnetic resonance imaging of the normal bone marrow. *Skeletal Radiol* 1998;27(9):471–483.
- Dwek JR, Shapiro F, Laor T, Barnewolt CE, Jaramillo D. Normal gadolinium-enhanced MR images of the developing appendicular skeleton. II. Epiphyseal and metaphyseal marrow. *AJR Am J Roentgenol* 1997;169(1):191–196.
- Burdiles A, Babyn PS. Pediatric bone marrow MR imaging. *Magn Reson Imaging Clin N Am* 2009;17(3):391–409, v.
- Cohen MD, Klatter EC, Baehner R, et al. Magnetic resonance imaging of bone marrow disease in children. *Radiology* 1984;151(3):715–718.
- Meyer JS, Siegel MJ, Farooqui SO, Jaramillo D, Fletcher BD, Hoffer FA. Which MRI sequence of the spine best reveals bone-marrow metastases of neuroblastoma? *Pediatr Radiol* 2005;35(8):778–785.
- Subhawong TK, Wilky BA. Value added: functional MR imaging in management of bone and soft tissue sarcomas. *Curr Opin Oncol* 2015;27(4):323–331.
- Fayad LM, Jacobs MA, Wang X, Carrino JA, Bluemke DA. Musculoskeletal tumors: how to use anatomic, functional, and metabolic MR techniques. *Radiology* 2012;265(2):340–356.
- Thawait SK, Marcus MA, Morrison WB, Klufas RA, Eng J, Carrino JA. Research synthesis: what is the diagnostic performance of magnetic resonance imaging to discriminate benign from malignant vertebral compression fractures? Systematic review and meta-analysis. *Spine* 2012;37(12):E736–E744.
- Del Grande F, Tatizawa-Shiga N, Jalali Farahani S, Chalian M, Fayad LM. Chemical shift imaging: preliminary experience as an alternative sequence for defining the extent of a bone tumor. *Quant Imaging Med Surg* 2014;4(3):173–180.
- Ahluwat S, Khandheria P, Subhawong TK, Fayad LM. Differentiation of benign and malignant skeletal lesions with quantitative diffusion weighted MRI at 3T. *Eur J Radiol* 2015;84(6):1091–1097.

12. Subhawong TK, Jacobs MA, Fayad LM. Diffusion-weighted MR imaging for characterizing musculoskeletal lesions. *RadioGraphics* 2014;34(5):1163–1177.
13. Chavhan GB, Alsabban Z, Babyn PS. Diffusion-weighted imaging in pediatric body MR imaging: principles, technique, and emerging applications. *RadioGraphics* 2014;34(3):E73–E88.
14. Herrmann J, Krstin N, Schoennagel BP, et al. Age-related distribution of vertebral bone-marrow diffusivity. *Eur J Radiol* 2012;81(12):4046–4049.
15. Zhang J, Cheng K, Ding Y, et al. Study of single voxel 1H MR spectroscopy of bone tumors: differentiation of benign from malignant tumors. *Eur J Radiol* 2013;82(12):2124–2128.
16. Fayad LM, Bluemke DA, McCarthy EF, Weber KL, Barker PB, Jacobs MA. Musculoskeletal tumors: use of proton MR spectroscopic imaging for characterization. *J Magn Reson Imaging* 2006;23(1):23–28.
17. Fukuda Y, Ando K, Ishikura R, et al. Superparamagnetic iron oxide (SPIO) MRI contrast agent for bone marrow imaging: differentiating bone metastasis and osteomyelitis. *Magn Reson Med Sci* 2006;5(4):191–196.
18. Atkin KL, Ditchfield MR. The role of whole-body MRI in pediatric oncology. *J Pediatr Hematol Oncol* 2014;36(5):342–352.
19. Darge K, Jaramillo D, Siegel MJ. Whole-body MRI in children: current status and future applications. *Eur J Radiol* 2008;68(2):289–298.
20. Goo HW. Regional and whole-body imaging in pediatric oncology. *Pediatr Radiol* 2011;41(suppl 1):S186–S194.
21. Padhani AR, Koh DM, Collins DJ. Whole-body diffusion-weighted MR imaging in cancer: current status and research directions. *Radiology* 2011;261(3):700–718.
22. Kumar J, Seith A, Kumar A, et al. Whole-body MR imaging with the use of parallel imaging for detection of skeletal metastases in pediatric patients with small-cell neoplasms: comparison with skeletal scintigraphy and FDG PET/CT. *Pediatr Radiol* 2008;38(9):953–962.
23. Bracken J, Nandurkar D, Radhakrishnan K, Ditchfield M. Normal paediatric bone marrow: magnetic resonance imaging appearances from birth to 5 years. *J Med Imaging Radiat Oncol* 2013;57(3):283–291.
24. Laor T, Jaramillo D. MR imaging insights into skeletal maturation: what is normal? *Radiology* 2009;250(1):28–38.
25. Jaramillo D, Laor T, Hoffer FA, et al. Epiphyseal marrow in infancy: MR imaging. *Radiology* 1991;180(3):809–812.
26. Emery JL, Follett GF. Regression of bone-marrow haemopoiesis from the terminal digits in the fetus and infant. *Br J Haematol* 1964;10(4):485–489.
27. Waitches G, Zawin JK, Poznanski AK. Sequence and rate of bone marrow conversion in the femora of children as seen on MR imaging: are accepted standards accurate? *AJR Am J Roentgenol* 1994;162(6):1399–1406.
28. Moore SG, Dawson KL. Red and yellow marrow in the femur: age-related changes in appearance at MR imaging. *Radiology* 1990;175(1):219–223.
29. Dunnill MS, Anderson JA, Whitehead R. Quantitative histological studies on age changes in bone. *J Pathol Bacteriol* 1967;94(2):275–291.
30. Byrd SE, Comiskey EM. Postnatal maturation and radiology of the growing spine. *Neurosurg Clin N Am* 2007;18(3):431–461.
31. Taccone A, Oddone M, Occhi M, Dell'Acqua AD, Ciccone MA. MRI “road-map” of normal age-related bone marrow. I. Cranial bone and spine. *Pediatr Radiol* 1995;25(8):588–595.
32. Sebag GH, Dubois J, Tabet M, Bonato A, Lallemand D. Pediatric spinal bone marrow: assessment of normal age-related changes in the MRI appearance. *Pediatr Radiol* 1993;23(7):515–518.
33. Ricci C, Cova M, Kang YS, et al. Normal age-related patterns of cellular and fatty bone marrow distribution in the axial skeleton: MR imaging study. *Radiology* 1990;177(1):83–88.
34. Sze G, Bravo S, Baiert P, Shimkin PM. Developing spinal column: gadolinium-enhanced MR imaging. *Radiology* 1991;180(2):497–502.
35. Dawson KL, Moore SG, Rowland JM. Age-related marrow changes in the pelvis: MR and anatomic findings. *Radiology* 1992;183(1):47–51.
36. Levine CD, Schweitzer ME, Ehrlich SM. Pelvic marrow in adults. *Skeletal Radiol* 1994;23(5):343–347.
37. Schweitzer ME, Levine C, Mitchell DG, Gannon FH, Gonnella LG. Bull's-eyes and halos: useful MR discriminators of osseous metastases. *Radiology* 1993;188(1):249–252.
38. Babyn PS, Ranson M, McCarville ME. Normal bone marrow: signal characteristics and fatty conversion. *Magn Reson Imaging Clin N Am* 1998;6(3):473–495.
39. Foster K, Chapman S, Johnson K. MRI of the marrow in the paediatric skeleton. *Clin Radiol* 2004;59(8):651–673.
40. Richardson ML, Lough LR, Shuman WP, Lazerte GD, Conrad EU. MR appearance of skeletal neoplasms following cryotherapy. *Skeletal Radiol* 1994;23(2):121–125.
41. Lonergan GJ, Cline DB, Abbondanzo SL. Sickle cell anemia. *RadioGraphics* 2001;21(4):971–994.
42. Vogler JB III, Murphy WA. Bone marrow imaging. *Radiology* 1988;168(3):679–693.
43. Pathria MN, Issacs P. Magnetic resonance imaging of bone marrow. *Curr Opin Radiol* 1992;4(6):21–31.
44. Gongidi P, Johnson C, Dinan D. Scurvy in an autistic child: MRI findings. *Pediatr Radiol* 2013;43(10):1396–1399.
45. Bowden DJ, Kilburn-Toppin F, Scoffings DJ. Radiology of eating disorders: a pictorial review. *RadioGraphics* 2013;33(4):1171–1193.
46. Guillerman RP. Marrow: red, yellow and bad. *Pediatr Radiol* 2013;43(suppl 1):S181–S192.
47. Carroll KW, Feller JF, Tirman PF. Useful internal standards for distinguishing infiltrative marrow pathology from hematopoietic marrow at MRI. *J Magn Reson Imaging* 1997;7(2):394–398.
48. Ruzal-Shapiro C, Berdon WE, Cohen MD, Abramson SJ. MR imaging of diffuse bone marrow replacement in pediatric patients with cancer. *Radiology* 1991;181(2):587–589.
49. Vesterby A, Myhre Jensen O. Aseptic bone/bone marrow necrosis in leukaemia. *Scand J Haematol* 1985;35(3):354–357.
50. Nies BA, Kundel DW, Thomas LB, Freireich EJ. Leukopenia, bone pain, and bone necrosis in patients with acute leukemia: a clinicopathologic complex. *Ann Intern Med* 1965;62:698–705.
51. Mitchell DG, Rao VM, Dalinka MK, et al. Femoral head avascular necrosis: correlation of MR imaging, radiographic staging, radionuclide imaging, and clinical findings. *Radiology* 1987;162(3):709–715.
52. Saini A, Saifuddin A. MRI of osteonecrosis. *Clin Radiol* 2004;59(12):1079–1093.
53. Janssens AM, Offner FC, Van Hove WZ. Bone marrow necrosis. *Cancer* 2000;88(8):1769–1780.
54. Tang YM, Jeavons S, Stuckey S, Middleton H, Gill D. MRI features of bone marrow necrosis. *AJR Am J Roentgenol* 2007;188(2):509–514.
55. Paydas S, Ergin M, Baslamisli F, et al. Bone marrow necrosis: clinicopathologic analysis of 20 cases and review of the literature. *Am J Hematol* 2002;70(4):300–305.
56. Macfarlane SD, Tauro GP. Acute lymphocytic leukemia in children presenting with bone marrow necrosis. *Am J Hematol* 1986;22(4):341–346.
57. Brown CH 3rd. Bone marrow necrosis: a study of seventy cases. *Johns Hopkins Med J* 1972;131(3):189–203.
58. Krishnan A, Shirkhoda A, Tehranzadeh J, Armin AR, Irwin R, Les K. Primary bone lymphoma: radiographic-MR imaging correlation. *RadioGraphics* 2003;23(6):1371–1383; discussion 1384–1387.
59. Linden A, Zankovich R, Theissen P, Diehl V, Schicha H. Malignant lymphoma: bone marrow imaging versus biopsy. *Radiology* 1989;173(2):335–339.
60. Kricun ME. Red-yellow marrow conversion: its effect on the location of some solitary bone lesions. *Skeletal Radiol* 1985;14(1):10–19.
61. Algra PR, Bloem JL, Tissing H, Falke TH, Arndt JW, Verboom LJ. Detection of vertebral metastases: comparison between MR imaging and bone scintigraphy. *RadioGraphics* 1991;11(2):219–232.

62. Yankelevitz DF, Henschke CI, Knapp PH, Nisce L, Yi Y, Cahill P. Effect of radiation therapy on thoracic and lumbar bone marrow: evaluation with MR imaging. *AJR Am J Roentgenol* 1991;157(1):87–92.
63. Stevens SK, Moore SG, Kaplan ID. Early and late bone-marrow changes after irradiation: MR evaluation. *AJR Am J Roentgenol* 1990;154(4):745–750.
64. Sacks EL, Goris ML, Glatstein E, Gilbert E, Kaplan HS. Bone marrow regeneration following large field radiation: influence of volume, age, dose, and time. *Cancer* 1978;42(3):1057–1065.
65. Cavenagh EC, Weinberger E, Shaw DW, White KS, Geyer JR. Hematopoietic marrow regeneration in pediatric patients undergoing spinal irradiation: MR depiction. *AJNR Am J Neuroradiol* 1995;16(3):461–467.
66. Otake S, Mayr NA, Ueda T, Magnotta VA, Yuh WT. Radiation-induced changes in MR signal intensity and contrast enhancement of lumbosacral vertebrae: do changes occur only inside the radiation therapy field? *Radiology* 2002;222(1):179–183.
67. Blomlie V, Rofstad EK, Skjøsberg A, Tverå K, Lien HH. Female pelvic bone marrow: serial MR imaging before, during, and after radiation therapy. *Radiology* 1995;194(2):537–543.
68. Libshitz HI, Cohen MA. Radiation-induced osteochondromas. *Radiology* 1982;142(3):643–647.
69. Roebuck DJ. Skeletal complications in pediatric oncology patients. *RadioGraphics* 1999;19(4):873–885.
70. Daldrup-Link HE, Henning T, Link TM. MR imaging of therapy-induced changes of bone marrow. *Eur Radiol* 2007;17(3):743–761.
71. Ecklund K, Laor T, Goorin AM, Connolly LP, Jaramillo D. Methotrexate osteopathy in patients with osteosarcoma. *Radiology* 1997;202(2):543–547.
72. Schwartz AM, Leonidas JC. Methotrexate osteopathy. *Skeletal Radiol* 1984;11(1):13–16.
73. Fletcher BD. Effects of pediatric cancer therapy on the musculoskeletal system. *Pediatr Radiol* 1997;27(8):623–636.
74. Fletcher BD, Wall JE, Hanna SL. Effect of hematopoietic growth factors on MR images of bone marrow in children undergoing chemotherapy. *Radiology* 1993;189(3):745–751.
75. Tanner SF, Clarke J, Leach MO, et al. MRI in the evaluation of late bone marrow changes following bone marrow transplantation. *Br J Radiol* 1996;69(828):1145–1151.
76. Rios AM, Rosenberg ZS, Bencardino JT, Rodrigo SP, Theran SG. Bone marrow edema patterns in the ankle and hindfoot: distinguishing MRI features. *AJR Am J Roentgenol* 2011;197(4):W720–W729.
77. Mizuta T, Benson WM, Foster BK, Paterson DC, Morris LL. Statistical analysis of the incidence of physeal injuries. *J Pediatr Orthop* 1987;7(5):518–523.
78. Jaramillo D, Shapiro F. Musculoskeletal trauma in children. *Magn Reson Imaging Clin N Am* 1998;6(3):521–536.
79. Lazzarini KM, Troiano RN, Smith RC. Can running cause the appearance of marrow edema on MR images of the foot and ankle? *Radiology* 1997;202(2):540–542.
80. Major NM, Helms CA. MR imaging of the knee: findings in asymptomatic collegiate basketball players. *AJR Am J Roentgenol* 2002;179(3):641–644.
81. Grampp S, Henk CB, Mostbeck GH. Overuse edema in the bone marrow of the hand: demonstration with MRI. *J Comput Assist Tomogr* 1998;22(1):25–27.
82. Barnett LS. Little League shoulder syndrome: proximal humeral epiphyseolysis in adolescent baseball pitchers—a case report. *J Bone Joint Surg Am* 1985;67(3):495–496.
83. Dwek JR, Cardoso F, Chung CB. MR imaging of overuse injuries in the skeletally immature gymnast: spectrum of soft-tissue and osseous lesions in the hand and wrist. *Pediatr Radiol* 2009;39(12):1310–1316.
84. Laor T, Wall EJ, Vu LP. Physeal widening in the knee due to stress injury in child athletes. *AJR Am J Roentgenol* 2006;186(5):1260–1264.
85. Rogers LF. The radiography of epiphyseal injuries. *Radiology* 1970;96(2):289–299.
86. Zbojniewicz AM, Laor T. Focal periphyseal edema (FOPE) zone on MRI of the adolescent knee: a potentially painful manifestation of physiologic physeal fusion? *AJR Am J Roentgenol* 2011;197(4):998–1004.
87. Scott RJ, Christofersen MR, Robertson WW Jr, Davidson RS, Rankin L, Drummond DS. Acute osteomyelitis in children: a review of 116 cases. *J Pediatr Orthop* 1990;10(5):649–652.
88. Dartnell J, Ramachandran M, Katchburian M. Haematogenous acute and subacute paediatric osteomyelitis: a systematic review of the literature. *J Bone Joint Surg Br* 2012;94(5):584–595.
89. Browne LP, Mason EO, Kaplan SL, Cassady CI, Krishnamurthy R, Guilleman RP. Optimal imaging strategy for community-acquired *Staphylococcus aureus* musculoskeletal infections in children. *Pediatr Radiol* 2008;38(8):841–847.
90. Jaramillo D. Infection: musculoskeletal. *Pediatr Radiol* 2011;41(suppl 1):S127–S134.
91. Averill LW, Hernandez A, Gonzalez L, Peña AH, Jaramillo D. Diagnosis of osteomyelitis in children: utility of fat-suppressed contrast-enhanced MRI. *AJR Am J Roentgenol* 2009;192(5):1232–1238.
92. Pugmire BS, Shailam R, Gee MS. Role of MRI in the diagnosis and treatment of osteomyelitis in pediatric patients. *World J Radiol* 2014;6(8):530–537.
93. Cohen MD, Cory DA, Kleiman M, Smith JA, Broderick NJ. Magnetic resonance differentiation of acute and chronic osteomyelitis in children. *Clin Radiol* 1990;41(1):53–56.
94. Falip C, Alison M, Boutry N, et al. Chronic recurrent multifocal osteomyelitis (CRMO): a longitudinal case series review. *Pediatr Radiol* 2013;43(3):355–375.
95. Manson D, Wilmot DM, King S, Laxer RM. Physeal involvement in chronic recurrent multifocal osteomyelitis. *Pediatr Radiol* 1989;20(1-2):76–79.
96. Fritz J, Tzaribatchev N, Claussen CD, Carrino JA, Horger MS. Chronic recurrent multifocal osteomyelitis: comparison of whole-body MR imaging with radiography and correlation with clinical and laboratory data. *Radiology* 2009;252(3):842–851.
97. Duffy CM, Lam PY, Ditchfield M, Allen R, Graham HK. Chronic recurrent multifocal osteomyelitis: review of orthopaedic complications at maturity. *J Pediatr Orthop* 2002;22(4):501–505.
98. Martel W, Holt JF, Cassidy JT. Roentgenologic manifestations of juvenile rheumatoid arthritis. *Am J Roentgenol Radium Ther Nucl Med* 1962;88:400–423.
99. Williams RA, Ansell BM. Radiological findings in seropositive juvenile chronic arthritis (juvenile rheumatoid arthritis) with particular reference to progression. *Ann Rheum Dis* 1985;44(10):685–693.
100. Schweitzer ME, White LM. Does altered biomechanics cause marrow edema? *Radiology* 1996;198(3):851–853.
101. Elias I, Zoga AC, Schweitzer ME, Ballehr L, Morrison WB, Raikin SM. A specific bone marrow edema around the foot and ankle following trauma and immobilization therapy: pattern description and potential clinical relevance. *Foot Ankle Int* 2007;28(4):463–471.
102. Pal CR, Tasker AD, Ostlere SJ, Watson MS. Heterogeneous signal in bone marrow on MRI of children's feet: a normal finding? *Skeletal Radiol* 1999;28(5):274–278.
103. Shabshin N, Schweitzer ME, Morrison WB, Carrino JA, Keller MS, Grissom LE. High-signal T2 changes of the bone marrow of the foot and ankle in children: red marrow or traumatic changes? *Pediatr Radiol* 2006;36(7):670–676.
104. Santori FS, Calvisi V, Manili M, Gambini A. Regional migratory osteoporosis. *Ital J Orthop Traumatol* 1985;11(3):371–380.
105. Tan EC, van de Sandt-Renkema N, Krabbe PF, Aronson DC, Severijnen RS. Quality of life in adults with childhood-onset of complex regional pain syndrome type I. *Injury* 2009;40(8):901–904.
106. Bruehl S. Complex regional pain syndrome. *BMJ* 2015;351:h2730.
107. Albazaz R, Wong YT, Homer-Vanniasinkam S. Complex regional pain syndrome: a review. *Ann Vasc Surg* 2008;22(2):297–306.